Weak Panel Zone Design in Steel Gabled Frames

Y. Shi & Y.Y. Chen
State Key Laboratory for Disaster Reduction in Civil Engineering, Tongji University, China

Y. Shi
Kyoto University, Japan

SUMMARY:
The widely used non-compact elements in steel gable frames induce different seismic behavior compared with that determined by the compact elements. By the conventional method the connection should be designed stronger than the beam and column members. Due to the local buckling of those members composed by non-compact elements in steel gabled frames, there will be no reliable component to efficiently consume energy input by earthquake. This paper presents a new view to design a weak connection. Two specimens with structural members composed of non-compact elements were tested. It was found that the specimen with a weak panel zone exhibited higher ductility and energy dissipating ability. A 3D finite element model was developed to supplement the test approach. The finite element results were firstly verified by comparing with experimental results which shows great satisfactory. Parametric studies were then performed to further explore feasibility of the weak panel zone design.

Keywords: thin-walled steel member, connection, local buckling, panel zone

1. INTRODUCTION

Steel gabled frames are commonly used for single story construction such as factory and warehouse buildings. Non-compact or slender elements are employed in the steel gabled frames' beam and column members to reduce the building's construction cost. Due to its light weight, the structure is subjected to relatively small earthquake load. However, the steel gabled frame can still be damaged by rare strong earthquake damage, as was found by an investigation after China's Wenchuan earthquake in 2008.

The general design theory tries to design the connection stronger than the connected members. The connected members are expected to be capable of extensive amounts of energy dissipation. It is believed that this type of a design can effectively prevent connection damage due to brittle failure. The connection damage is undesirable because it can result in local or global collapse. However, this design method is not necessarily a benign event in the steel gabled frame. The usage of a non-compact or slender element in steel gabled frames causes the members and connections to behave differently. The members will buckle instead of experiencing plastic failure. In that case, if the connection is designed too strong, as in special moment frames (AISC 2005), there is no reliable component in the steel gabled frame to efficiently consume the energy input from an earthquake ground motion. On another hand, the panel zone (PZ) is also at risk of buckling under little shear if no stiffener is placed in the PZ. The shear buckling of the PZ produces out-of-plane deformation, and this deformation mode will dissipate part of the energy. Though such an energy dissipation mode has been considered unstable, it has not been thoroughly studied. Considering the fact that the member in a single story steel gabled frame plays the same role as the connection, i.e., the failure of either the member or the connection will cause the structure to collapse; both the beam or column member and the connection have the potential to dissipate the earthquake input energy.

To evaluate the seismic behavior of the connection in steel gabled frames, two specimens with end plate connections connecting the beam and the interior column of a steel gabled frame composed of non-compact elements under cyclic loads were tested. A 3D solid element model was developed and parametric study was conducted to further study the hysteretic behavior of the weak PZ design.

2. TEST PROGRAM

2.1. Specimen Design

Two beam-to-interior column connection specimens were designed from the prototype connection, where the column and beam section was scaled from the prototype with a factor of 2/3, as shown in Table 2.1 and Fig. 2.1. Two beams were connected to the flanges of a column at two sides by end plates. Because the angle between the centroidal axis and the flange of the beam in the prototype is small (1/30), the designed beam had a uniform section and was perpendicular to the column to make the setup process easier. By verifying the PZ configuration the specimens were designed to evaluate the behaviors of two failure modes: column buckling and PZ buckling. In this respect, welds and bolts were designed to be stronger than the other components in the specimen to avoid brittle failure. Fillet welds were adopted, except for the joints between the end plate and the beam and column members, which were welded by a completely penetrated weld. According to AISC 2005, the cross sections of the columns have a non-compact web and a compact flange.

The column and PZ were two weak components of the specimens in the design. The ultimate buckling moment M_u^c of column can be calculated from Eqn. 2.1 (Chen et al. 2006).

$$M_u^c = b_{cf} t_{cf} (h_c - t_{cf}) f_{cf} + 0.5 h_{ce} t_{cw} f_{cw} (h_{cw} - 0.5 h_{ce}) \quad (2.1)$$

where f_{cf} and f_{cw} are the yield strength of column flange and web; b_{cf}, t_{cf}, h_c, h_{cw}, t_{cw} and h_{ce} are the column flange width, column flange thickness, column depth, column web depth, column web thickness and effective web depth. The effective web depth is assigned to be $60t_{cw}(235/f_{cw})^{0.5}$.

Theoretical predictions of the ultimate shear resistance of the PZ can be made in accordance with tension field theory, developed by Evans (1983). The ultimate moment of the PZ without diagonal stiffener can be calculated from Eqn. 2.2.

$$M_u^{pz} = h_{cw} L_b L_{lp} V_u / (L_b L_{lp} - h_{cw} L_{lb}) \quad (2.2)$$

where L_b, L_{lp} and L_{lb} are the beam length, distances from loading point to beam flange and beam centreline; V_u is ultimate buckling resistance of the PZ without diagonal stiffener calculated from Evans (1983). For specimen B1-1, buckling of PZ is not considered and the ultimate moment of PZ can be calculated from Eqn. 2.3

$$M_u^{pz} = h_{cw} L_b L_{lp} h_{bw} t_{pz} \tau_{pz} / (L_b L_{lp} - h_{cw} L_{lb}) + 2 A_s f_{ys} h_{cw} \sin\alpha \quad (2.3)$$

where h_{bw}, t_{pz}, τ_{pz}, A_s and f_{ys} are beam web depth, thickness of PZ, shear strength of PZ, cross section area and yield strength of the diagonal stiffener; α represents the angle between the stiffener and beam flange.

Table 2.1. Geometrical Features of the Specimens

Specemen ID	EW/T[a] of			Diagonal stiffener in PZ	Bolt Diameter (mm)	$\eta = M_u^c / M_u^{pz}$	Calculated capacity (kN)
	Column web	Column flange	PZ				
B1-1	137	10.3	170	Yes	16	0.69	155
B1-2	137	10.3	170	No	16	1.06	148

Note: [a]EW/T is the effective width-to-thickness ratio and is defined as $h_w/t_{cw}\,(f_{cw}/235)^{0.5}$ for column web or PZ

and $b_{cf}/2t_{cf}\,(f_{cf}/235)^{0.5}$ for column flange, where h_w is the column web height for column web or beam web height for PZ.

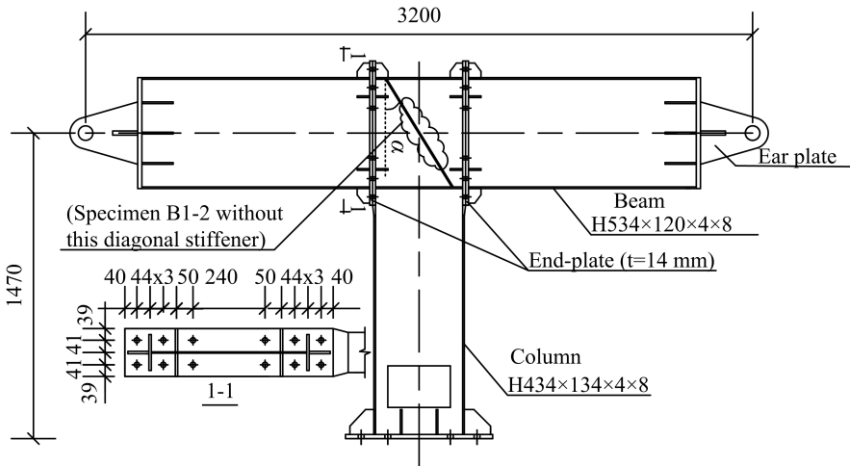

Figure. 2.1. Test specimens

All of the specimens were made of Q345B steel according to the Chinese GB standards, and the Grade 10.9 high-strength bolts with pre-tension designed as a slip critical type joint were used. The mechanical properties of the steel plates and bolts can refer to Shi et al, 2012.

2.2. Setup and Loading System

The test setup was designed to accommodate specimens with columns in a horizontal position for ease of loading, as shown in Fig. 2.2. The two ends of the beam were connected to the ground and reaction frame by pins.

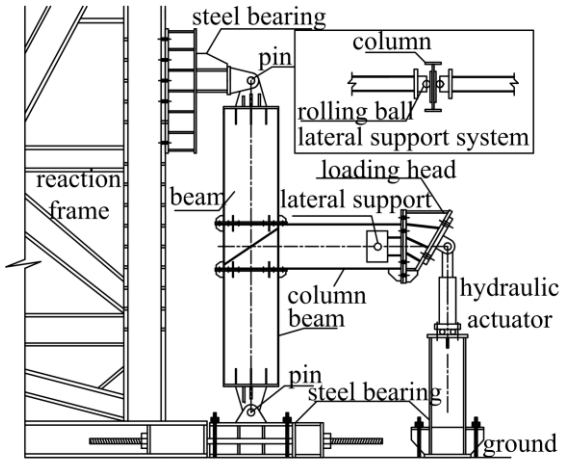

Figure 2.2. Test setup

The lateral load was applied to the cantilever end of the column via a hydraulic actuator at a distance of 1900 mm from the beam centerline. The loading process followed a displacement control program, with a stepwise-increasing deformation at the loading point. Each incremental displacement step was 5 mm, and there was one loading cycle for each step. No axial load was applied to the column because there is only a small amount of axial force in the actual column members of light weight steel gabled frames. To prevent the out-of-plane movement of the specimens, a lateral support system was provided near the column end.

To interpret the general behavior of the specimen and therefore evaluate the energy dissipating ability

of the connection, the concept of sub-assemblage is utilized; those parts of the specimen will develop non-linear deformation in test is used through this paper. The rotation of sub-assembly θ_s can approximately be determined by Eqn. 2.4. The instrument information can be found in Shi et al. 2012.

$$\theta_s = \Delta_p / L_{lp} \tag{2.4}$$

where Δ_p is the column end displacement excluding the elastic deformation caused by column and beam; and L_{lp} is the distance from column end to end plate.

2.3. Test Results

Figure 2.3 shows the deformation of two specimens after failure. For specimen B1-1, column flanges yielded at the 20 mm cycle, and eventually resulted in local buckling of the column web and flange. The measured strain indicated that plastic deformation occurred in the PZ at 20 mm cycle and visible buckling deformation was detected at the same loading cycle. However, the diagonal stiffener prevented the further development of the local buckling in the PZ. Without the diagonal stiffener, the PZ of specimen B1-2 yielded completely at the 15 mm cycle and resulted in visible buckling of the PZ at the same cycle. During the test the convex wave of buckling deformation of PZ changed its direction from one side to another periodically with the reverse of shear force, accompanying with loud sound. Further loading after the buckle of PZ resulted in the yielding of column at 20 mm cycle, and local buckling of both column flange and web at the 25 mm cycle. The test on B1-2 shows that the PZ was able to sustain high loading demands even after shear buckling happened. Neither failure of the bolt nor weld was observed for the two specimens during the tests. The ultimate capacity is shown in Table 2.2. Comparing with the calculation results shown in Table 2.1, it can be seen Eqn. 2.1 and 2.2 are accurate.

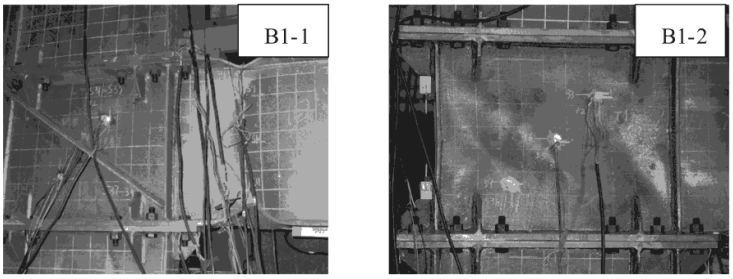

Figure 2.3. Deformation after failure

The hysteretic curves of moment vs. sub-assemblage rotation (M-θ_s) of the two specimens are shown in Fig. 2.4, where the moment M is taken as the moment at the neighboring beam flange. The area encircled by the hysteretic curves for each specimen represents the energy dissipated by the sub-assemblage of the whole specimen. As marked in the figure, column buckling happened both in the two specimens before reaching to the maximum capacity. Due to the buckling behavior of the column the strength deterioration occurred for both specimens.

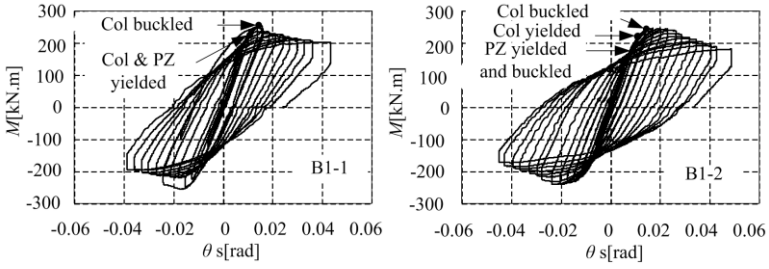

Figure 2.4. Moment-rotation relationship (Col: column)

The ductility of PZ and sub-assemblage can be quantified by the index, μ, defined as Eqn. 2.5 (Shi et al. 2012) from the M-θ (θ_s) relationship.

$$\mu=\theta_m/\theta_y \tag{2.5}$$

where θ_m relates the ultimate rotation corresponding to a decrease in the load to 85% of the maximum load in each experiment and θ_y is the yield rotation calculated from the yield capacity and initial stiffness. The calculation results in both two loading directions are shown in Table 2.2. It can be seen that the ductility of specimen B1-2 is much larger than that of specimen B1-1, which indicates that the PZ is a very ductile element and its inelastic deformation can help improve the ductility of the specimen.

The cumulative energy dissipated by the sub-assemblage for all the loading cycles before the load decreased to 85% of the maximum was calculated and shown in last column of Table 2.2. It can be seen that the specimens B1-2 dissipated more energy than that by specimen B1-1. This shows that the inelastic deformation of the PZ after local buckling could improve the energy dissipation capacity of the specimen.

The amount of energy dissipated by PZ and column member in specimen B1-2 corresponding to each loading cycle is given in Fig. 2.5. As shown in the Figure, most of the total energy was dissipated by PZ before the load reaching maximum (at the 40 mm cycle). This proves that the PZ had a stable energy dissipating capacity before strength deterioration. And although the total energy dissipated increased after the column reaching its ultimate strength, the strength decreased seriously.

Table 2.2. Test Results

Specimen ID	Ultimate capacity (kN)	μ^+	μ^-	Cumulative Energy (kN.m)
B1-1	155	2.6	1.7	9.7
B1-2	150	4.1	3.9	44.4

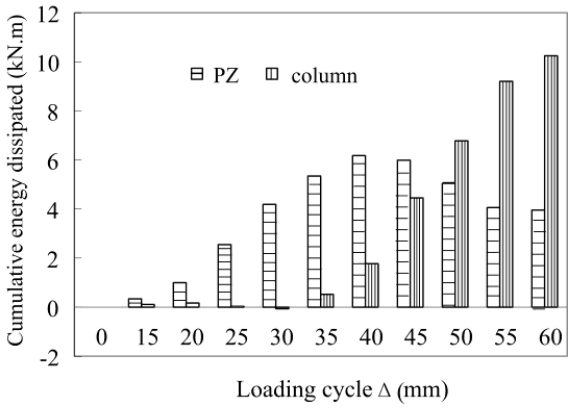

Figure 2.5. Cumulative energy dissipation of specimen B1-2

Based on the conclusion from the test, a weak PZ design could improve the seismic behavior of single story steel gabled frame with non-compact elements. To further investigate the weak PZ design, the FE method was used in this paper.

3. FE ANALYSIS

3.1. FE Model and Validation

The FE analysis was carried out by using ANSYS 9.0 package. All elements of the beams, columns, end plates, stiffeners and the high strength bolts were modeled by the ANSYS first-order solid

hexahedral element SOLID45. The interface between the end plate and the beam (or column) flange was modeled by the 3D target surface element TARGE170 and the surface-to-surface element CONTA174. Fig. 3.1 shows a typical FE model of a specimen, and that of end plate and a high strength bolt.

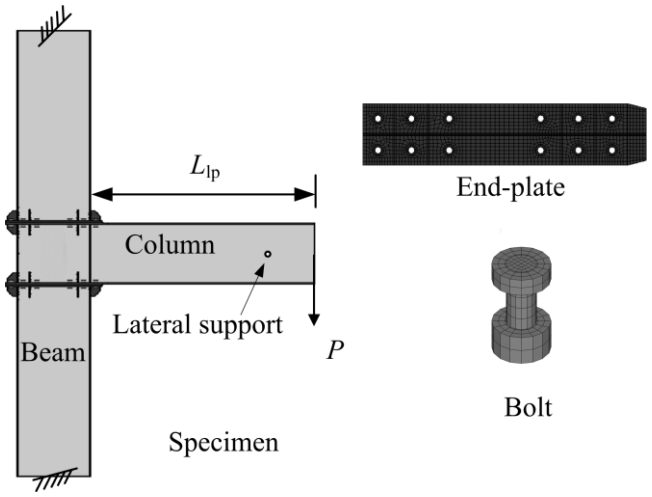

Figure 3.1. FE model

The FE models for two specimens tested were established. The boundary conditions of the FE model were set as follows: the nodes at the middle height of the two beam end sections were fixed to simulate the pin connections; The loading head apparatus on the cantilever end of column was replaced by an extended column segment, and the end load was applied on the node at the middle height of the column end section. Out-of-plane displacement was restrained at the same position of the test in order to simulate the lateral support used in the tests.

A kinematic hardening model based on Von-Mises yield criterion was adopted. The stress-strain relationship of the steel used in the FE analysis was assumed to be a multi-line model as illustrated in Fig. 3.2. The yield stress f_y and tensile stress f_u for the model were the same as the test data. Elastic modulus E and Poisson's coefficient in elastic stage were taken as 2.06×10^5 MPa and 0.3, respectively. The strain ε_{st} of column, beam, end plate and stiffeners was set as 0.012. The tangent modulus of hardening stage was supposed as 1.5% of the initial modulus up to ε_u. For bolt steel (Fig. 3.2b) the tangent modulus for hardening was set as 10% of the initial modulus.

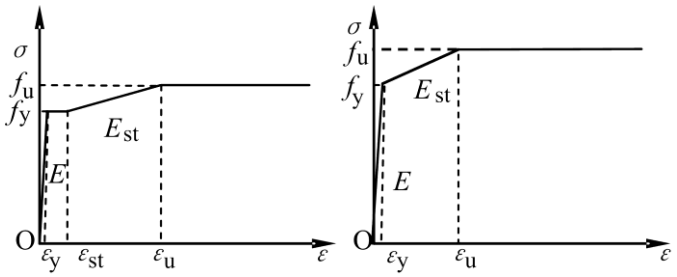

Figure 3.2. Stress-strain relationship: (a) steel and (b) bolt

3.2. Comparison of Results from FE Analysis and Tests

Fig. 3.3 shows the comparison of deformation modes at the ultimate load. In addition, the comparison of the moment-rotation curves of specimen B1-2 is shown in Fig. 3.4. The comparisons indicate that the FE model could simulate the test results satisfactorily. Hence the FE model established was reliable and accepted for further analysis.

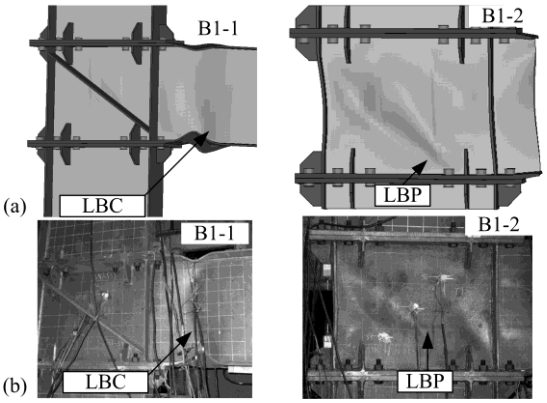

Figure 3.3. Deformation modes: (a) FE and (b) test

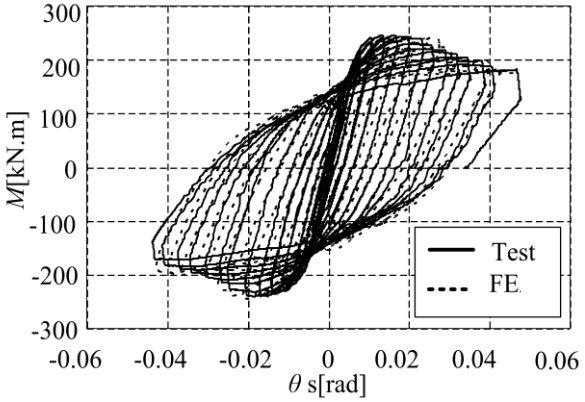

Figure 3.4. Moment-rotation relationship

3.3. Parametric Analysis

The parametric analysis placed the emphasis on the weak PZ design aimed at improving the seismic behavior of light weight steel gabled frame. The beam and column sections of FE models were H600×134×6×8 mm and H466×146×6×8 mm, respectively. The total beam length and the distance from the loading point to the centerline of the beam was taken as 16.93 m and 5.34 m, respectively, as scaled from the prototype, which was not possible in the physical test. Totally eleven specimens were designed as shown in Table 3.1 and could be categorized into three different groups in which the specimens had same column and beam sections. Different column capacity to PZ capacity ratios (η= M_u^c/ M_u^{pz}) from 0.62-1.28 were adopted as shown in the table. Also, different end plate positions were also included.

Table 3.1. Design of Specimens

Specimen ID[a]	Group	EW/T of		Yield strength of column	Diagonal stiffener	η
		Column web	PZ			
C6B6E18HO	I	91	118	345	No	0.86
C6B6E18HW		91	118	345	Yes	0.62
C6B4E18HO_1	II	91	177	345	No	1.28
C6B4E18HO_2		91	177	322	No	1.20
C6B4E18HO_3		91	177	310	No	1.16
C6B4E18HW		91	177	345	Yes	0.81
C4B4E18HO_1	III	136	177	390	No	1.20
C4B4E18HO_2		136	177	375	No	1.16
C4B4E18HO_3		136	177	345	No	1.06
C4B4E18HW		136	177	345	Yes	0.67
C4B4E12VO		136	177	345	No	1.07

Note: [a] The numbers following the letters C, B, E of the specimen ID represent the thickness of column web, beam web and PZ in mm; the letter H or V refers to end plate position at column top or beam end (as in the test), and the letter W or O represents whether the specimen has the diagonal stiffener or does not.

The stress-strain relationships for the steel plates and bolts were represented by elastically-perfect plastic model. The yield strength of PZ was 345 MPa and the yield strength of column elements varied as shown in Table 3.1. All the bolts used were M20, Grade 10.9 high strength bolts with pre-tension designed as slip critical type joint. The yield strength of bolts was the same as in the FEM analysis for validation. In order to prevent the flexural-torsional buckling of the specimen, the out-of-plane displacement of one node at the middle of the column and two beams was restrained. Cyclic loading path was adopted to evaluate the seismic behavior of the specimens. By comparison of different loading increments it was found that a 30 mm column end incremental displacement per loading cycle was fine smaller enough to achieve stable strength deterioration.

Fig. 3.5 shows three typical deformation modes. No bolt failure was found in the simulation. LBC and

LBP represent local buckling of column and local buckling of PZ, respectively. Fig. 3.6 shows the moment-rotation relationship of three specimens with typical deformation modes.

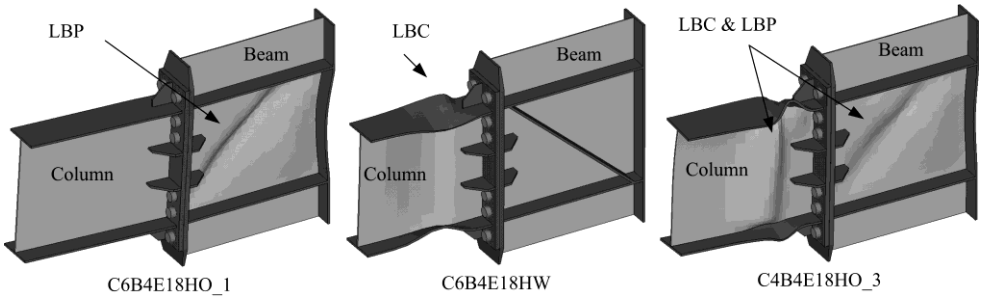

Figure. 3.5. Deformation modes

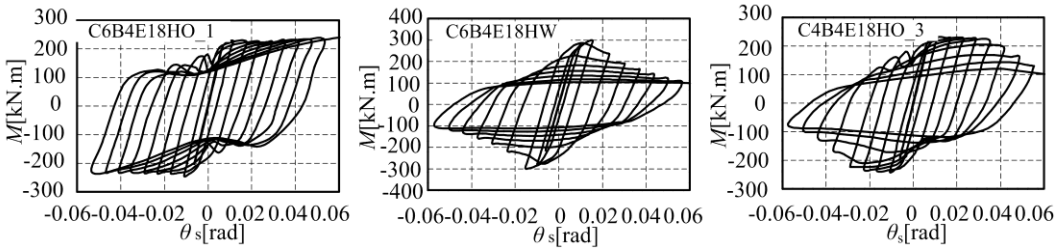

Figure 3.6. Moment-rotation relationship

The ductility of sub-assemblage of all the specimens was calculated by Eqn. 2.5 and shown in Table 3.2. The cumulative energy dissipation before the specimen's resistance decreased to 80% of the maximum is also shown in this table. For specimens that the resistance did not decrease to 80% of the maximum the dissipated energy was calculated up to the loading cycle of 300 mm.

It is seen from Table 3.2 that the coefficient μ was much higher for those specimens with LBP mode compared with the specimens with LBC mode. The usage of diagonal stiffener prevented the shear buckling of PZ and increased the ultimate capacity. However, the ductility of specimen decreased significantly once the unfavorable LBC mode happened prior to LBP, referring to specimens C6B4E18HW and C4B4E18HW.

The comparison within group I shows that those two specimens had similar ductility and energy dissipation capacity since only local buckling of column happened for both specimens. The thickness of PZ in group II was thinner than that in group I. Decreasing the PZ thickness made the PZ more flexible if no stiffener was added. The ductility and energy dissipation capacity were increased due to the local buckling of PZ. The difference between specimens C4B4E12VO and C4B4E18HO_3 was the end plate position. It is found that specimen C4B4E12VO had better energy dissipation capacity compared with C4B4E18HO_3 because the LBC mode in the latter was more predominant. The specimen C4B4E12VO had stronger support around the PZ which enabled the PZ to develop its inelastic deformation.

The calculation results indicate the deformation modes of the specimen depended on the column capacity to PZ capacity ratio η. If η was greater than 1.2, only the PZ bucked. If η was greater than 1.06 but smaller than 1.16, both PZ and column buckled. And if η was smaller than 0.86, only column buckled. The ductility and amount of energy dissipation of the specimen depended on the column capacity to PZ capacity ratio η, rather than the column web or PZ effective width to thickness ratio. Those specimens with same end plate configuration and similar η were found to have similar ductility and energy dissipation (C6B6E18HO vs. C6B4E18HW, C6B4E18HO_3 vs. C4B4E18HO_2, and C6B4E18HO_2 vs. C4B4E18HO_1).

Table 3.2. FE Calculation Results

Specimens ID	Deformation modes	M_u^{FE} (kN.m)	M_u^{EQ} (kN.m)	μ^+	μ^-	Energy dissipation (kN.m)		
						PZ	Column	Sub-assemblage
C6B6E18HO	LBC	295	277	2.4	2.2	1	20	21
C6B6E18HW	LBC	296	277	2.3	2.5	0	21	22
C6B4E18HO_1	LBP	243	217	7.1	7.1	124	2	126
C6B4E18HO_2	LBP	234	217	7.2	6.9	128	4	132
C6B4E18HO_3	LBC& LBP	230	217	7.3	7.0	119	1	120
C6B4E18HW	LBC	298	277	2.5	2.3	2	18	20
C4B4E18HO_1	LBP	237	217	6.8	6.6	133	3	136
C4B4E18HO_2	LBC& LBP	236	217	7.0	6.7	119	4	123
C4B4E18HO_3	LBC& LBP	230	217	5.5	4.0	40	6	46
C4B4E18HW	LBC	257	232	2.0	1.8	0	9	9
C4B4E12VO	LBC& LBP	224	215	7.4	6.9	92	7	99

The above discussion reveals that the LBP mode is a stable deformation mechanism which can provide high ductility and energy dissipation capacity. Therefore it can be used in seismic design for the single story steel gabled frame composed of members with non-compact o elements. More FE parametric analysis is needed to develop a design formula. The influence of stiffness should also be considered.

4. CONCLUSION

Two specimens with structural members composed of non-compact elements were tested. It was found that the specimen with a weak PZ exhibited higher ductility and energy dissipating ability. A 3D finite element model was developed to supplement the study. The finite element results were firstly verified by comparing with experimental results. Parametric studies were then performed to further explore feasibility of the weak PZ design. Relatively low ductile behavior and energy dissipation capacity were observed for the deformation mode of LBC, whereas the deformation modes of LBP and LBP & LBC exhibited stable hysteretic behavior, relatively high ductile behavior and energy dissipation capacity. The diagonal stiffener in the PZ could improve the ultimate capacity but decreased the ductility and energy dissipation capacity and therefore it is recommended that the diagonal stiffener should not be installed.

The calculation results indicate the deformation modes of the specimen depend on the column capacity to PZ capacity ratio. By carefully setting this ratio the LBP or LBP & LBC deformation mode will occur. It is recommended that the end plate should be placed at beam end so that the end plates can provide stronger support to the PZ.

AKCNOWLEDGEMENT
This research is financially supported by NSF of China, with project number of 51038008.

REFERENCES

AISC. (2005). Seismic Provisions for Structural Steel Buildings, ANSI/AISC 341-05, American Institute of Steel Construction, Inc., Chicago, IL.

Chen, Y, Wu, X, Tian, H, Zhao, J. and Ma, Y. (2006). Experiment of non-compact H-shaped members and frames subjected to cyclic loads and the prediction of capacities, *Steel Structures*. **6**, 215–226.

Evans, H. R. (1983). Longitudinally and transversely reinforced plate girders. Plated structures, stability and strength, R. Narayanan, ed., Elsevier Applied Science, London, 1–37.

Shi, Y, Chen, Y.Y, Xu, Y. and Zhao, X.Z (2012). Experimental analysis on the local buckling behavior at panel zone of beam-to-column connection in steel gabled frames, *7th International conference on Advances in Steel Structures*. Vol. 1, 443-451.